

FEM modeling of lean duplex stainless steel welding

Z. Brytan ^{a,*}, J. Niagaj ^b, W. Pakieła ^a, M. Bonek ^a

^a Institute of Engineering Materials and Biomaterials, Mechanical Engineering Faculty, Silesian University of Technology, Str. Konarskiego 18a, 44-100 Gliwice,

^b Institute of Welding, ul. Bł. Czesława 16-18, 44-100 Gliwice, Poland

* Corresponding e-mail address: zbigniew.brytan@polsl.pl

ABSTRACT

Purpose: Investigations include finite element model FEM of the various weld test performed on lean duplex stainless steels (TIG, MIG) and study calculated heat thermal cycle and deriving parameters.

Design/methodology/approach: The FEM model was also applied to evaluate residual stress on the weld surface. The accuracy of the FEM model was verified by comparing the results of the computer simulation of the stresses with experimental results.

Findings: Obtained result can be correlated to measured ferrite content in the weld, thus providing a simple prediction of phase balance in weld microstructure dependent on introducing heat input. Comparative analysis of the numerical FEM calculations and residual stress measurements made by X-ray diffraction showed good correlation.

Practical implications: Numerical calculations allow to quick selection of the optimal welding process parameters. Analysis of the thermal cycles curves has enabled to determine the basic parameters such as maximum temperature, heating time and cooling down and the rate of temperature is reached maximum and intermediate temperature ranges important for phase transformations.

Originality/value: A computer simulation of the stresses was carried out in the ANSYS environment using the FEM method.

Keywords: Lean duplex; Stainless steel; Heat input; FEM; Residual stress

Reference to this paper should be given in the following way:

Z. Brytan, J. Niagaj, W. Pakieła, M. Bonek, FEM modeling of lean duplex stainless steel welding, Journal of Achievements in Materials and Manufacturing Engineering 70/1 (2015) 36-44.

ANALYSIS AND MODELLING

1. Introduction

Lean duplex stainless steel (LDSS) becomes increasingly used in welded load bearing constructions. The higher strength of lean duplex stainless steel allows thinner sections of LDSS to replace components made with thicker sections of standard austenitic Cr-Ni and Cr-Ni-Mo

stainless steel alloys. This substitution may result in considerable cost savings. The high strength, toughness, corrosion resistance, and weldability of lean duplex stainless steel family makes them a good choice for use in many industrial branches [1-4].

One of the main problems concerning duplex stainless steels is a proper ferrite-austenite ratio, that can change due

to rapid cooling associated with weld thermal cycles resulting in excessive content of ferritic phase. The predominance of ferrite in the weld resulting in the loss of strength and increased susceptibility to intergranular corrosion. The weld microstructure and the austenite to ferrite ratio are largely influenced by welding heat inputs and the cooling rates from welding temperature. Consequently, a careful balance of heat input and cooling rates must be selected in order to achieve a favourable phase balance and avoid the formation of a coarser grained microstructures in the weld [1-7].

The FEM is broadly applied to simulate different welding processes, where the welding pole shape, the Marangoni effect, the welding distortion, the thermal stress, the heat thermal cycle, the residual stress distribution, the welding temperature fields can be predicted [9-14]

The X-ray diffraction technique is widely used for the determination of surface stresses [1-4]. One of the main advantages of diffraction methods is the possibility to obtain separate measurements for each phase of the material, so for ferrite and austenite, separately. Regarding duplex stainless steel the X-ray diffraction techniques were usefully applied to evaluate residual stresses in welded joints [1-8].

2. Experimental procedure

The present studies were performed on lean duplex stainless steel grade UNS S82441 sheet of the thickness 6.0 mm, with the chemical composition presented in the Table 1. The Pitting Resistance Equivalent Number PREN calculated according to the formula: $PREN = \%Cr + 3.3 \times (\%Mo) + 16 \times (\%N)$ for a given melt is equal to $PREN = 33.7$. The (Cr/Ni) equivalent ratio for giving composition was 4.4. During TIG welding respective shielding gases were applied: pure Ar, the mixes of Ar+N₂ (5, 10 and 15 %), a mixture of Ar and He in the relation 50/50.

Table 1.
Chemical composition of lean duplex stainless steel UNS S82441

Chemical composition, wt. %									
C	Si	Mn	P	S	Cr	Ni	Mo	Cu	N
0.025	0.36	3.00	0.022	0.001	23.92	3.66	1.61	0.39	0.279

The welding joints were produced using sheet plates grade S82441 with the dimensions 100x50x6 mm on the TIG mechanized welding stand consisting of welding source power Lorch V40, a welding trolley Promotech

DC20 with the precisely adjustable travel speed of torch and an attachment device to position welded pieces. The welding speed of all samples was constant and the current intensity was changed in the range from 50 to 300 A resulting in heat input 0.11÷1.17 kJ/mm.

Additionally the various parts of the sample surface were treated in a variety of ways prior to corrosion testing: 1) etching (abbreviation E) with a commercially available etching paste, 2) cleaning with a wire brush (abbreviation B+E), and then etched with the paste, 3) machining (abbreviation M) by milling surface layer removing depth of 0.1 -0.3 mm (max. 0.5 mm) from the face of the weld. The milling was applied in aim to mechanically remove of oxides and other surface contamination that might occur on the surface of the weld face and would not be removed by brushing and pickling treatment.

The microstructural characterization was performed on the cross-section of welded samples. Microstructure observations and geometrical characteristics of weld bead were carried out in the light and scanning electron microscope. Light microscope observations involved etching using Aqua Regia reagent and were performed at 400x and 1000x magnifications using a LEICA MEF4A microscope to evaluate phase content.

Stresses for the analysed welds were measured with the $g\text{-sin}^2\psi$ method with X'Pert Stress Plus software with values of material constants provided in a database indispensable for calculations. The $\text{sin}^2\psi$ method is mainly based on the effect of diffraction line displacement for different ψ angles, which occur in the stress conditions of materials that have a crystalline structure, and a silicon strip detector that is applied at the side of the diffracted beam. The inclination angle ψ of the test pieces is modified within a range of 0°–75° towards the primary beam. The stress analysis was performed in the transverse direction of the welded joint.

3. Results and discussion

The austenite and ferrite content, in studying welds was measured based on metallographies observation, according to ASTM E562 standard by systematic manual point count to determine the volume of observed phases. The phase measurement was performed on a cross section of the weld, near weld surface (Tab. 2). The influence of the heat input increase in the austenite content is evident on autogenous TIG welding. Nitrogen presence in the shielding gas negligible influenced austenite content at low heat input and low nitrogen content (5%N₂), but its influence is evident for high heat input and high nitrogen content. TIG

welding in Ar+He shielding gas mixture shows the same austenite content as for autogenous TIG welding for comparable heat input. The A-TIG weld compared to TIG weld shows higher austenite content when comparing the same heat input.

The finite element model (FEM) computations were performed using ANSYS software. The scope of FEM simulation was the determination of temperature distribution during welding process at various process configurations regarding heat input and welding method.

The finite element model (FEM) computations were performed using ANSYS software. The scope of FEM simulation was the determination of temperature distribution during welding process at various process configurations regarding heat input and welding method.

During this investigation, the process of welding of a butt-weld joint of two lean duplex stainless steel plates is simulated by the 3-D FEM (Finite Element Method). During the FEM analysis of welding process was performed heat transfer analysis and residual stress analysis. The dimension of the welding's plates used in the simulations was 50x100x6mm. Due to stress gradients and high temperature in the weld area, the finite element model has a relatively fine mesh in remelted zone and heat affected zone. In the remainder parts of the model was used a slightly larger mesh to increase the speed of calculation. In the applied model for the simulated thermal and structural phenomena was using two different elements. For thermal analysis was used the element type SOLID70 which has eight nodes with a single degree of freedom, temperature, at each node. This type of element has a three-dimensional thermal conduction capability. For the structural analysis (residual stress) in the model was used SOLID45 that is designed for the three-dimensional modelling of solid structures. This element has eight nodes having three degrees of freedom at each node. The model assumed nonlinear changes of thermal and mechanical properties as a function of temperature. The heat input during the welding process is modelled in the FEM

simulation by the heat flux calculated on the basis of voltage and current welding process, the speed of the head during the welding and efficiency. In the model was assumed transferring heat from the sample surface after removal of the heat flux by convection and radiation.

In order to simulate moving heat source it is necessary to model the heat source during each time increment. The analysis used a simplified moving heat source by assuming that the welding arc stayed at an element with constant specific volume heat flux and then moved to the next element at the end of the load step.

Three-dimensional map of the residual stress and thermal distribution were presented for autogenous TIG welding at heat input 0.45 kJ/mm on the Fig. 1. Comparative analysis of temperature distribution maps obtained on the basis of FEM simulation with the length and depth of solidified molten pool obtained during the welding process shows good compatibility of the results. FEM simulation of the liquid molten pool shape and temperature distribution during the process was shown in the Figs. 2 and 3. The depth values obtained in simulation are very close to experimental data. Regarding the shape of molten pool the higher differences have been noted. The heat flux input considered in the simulation is only part of the mechanism for heating, thus the final shape of solidified molten pool will be depended strongly depend on more variables, especially the shielding gas composition, where the specific shape of the weld is obtained when using i.e. He addition to Ar atmosphere. The TIG welding (autogenous and with shielding argon and argon-nitrogen atmosphere) where a flat shape of molten pool is produced and is becoming deeper, but still having a circular shape applied FEM model is able to predict very closely the real molten pool dimensions (width and depth). Where during TIG welding a helium is applied or an activated flux (A-TIG) and penetration deep is increased as well as specific shape of molten pool is obtained applied FEM model not proven realistic comparison with the experimental data.

Table 2.

The welding parameters and ferrite content in the weld of TIG and A-TIG welded lean duplex stainless steel UNS S82441

Current, A	Parent metal	Ferrite content, % / Heat input, kJ/mm					A-TIG
		TIG					
		Ar	Ar+5%N ₂	Ar+10%N ₂	Ar+15%N ₂	Ar+He	
50	45 / -	80-75 / 0.11	-	-	-	-	-
100		80-75 / 0.27	75-70 / 0.26	70-65 / 0.26	65-60 / 0.26	-	60-55 / 0.29
150		75-70 / 0.45	70-65 / 0.42	70-65 / 0.44	60-55 / 0.43	-	60-55 / 0.48
200		70-65 / 0.65	70-65 / 0.65	65-60 / 0.65	60-55 / 0.65	30-35 / 0.72	55-45 / 0.68
250		65-60 / 0.89	-	-	-	-	-
300		60-55 / 1.17	-	-	-	-	-

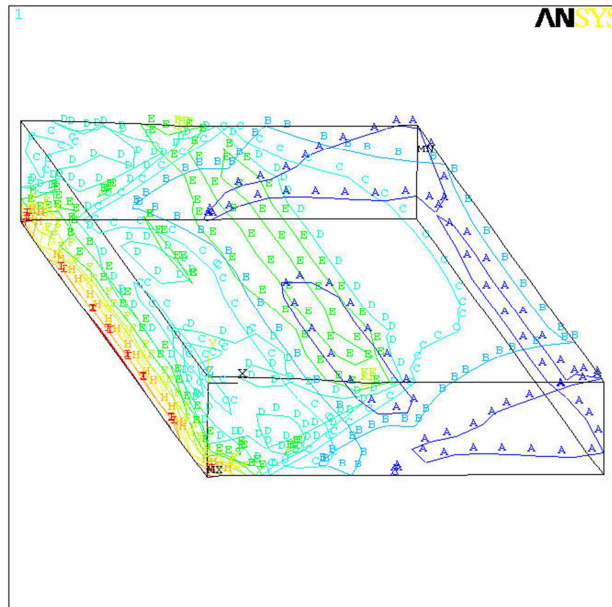


Fig. 1. Three-dimensional distribution of residual stress after autogenous TIG welding at heat input 0.45 kJ/mm

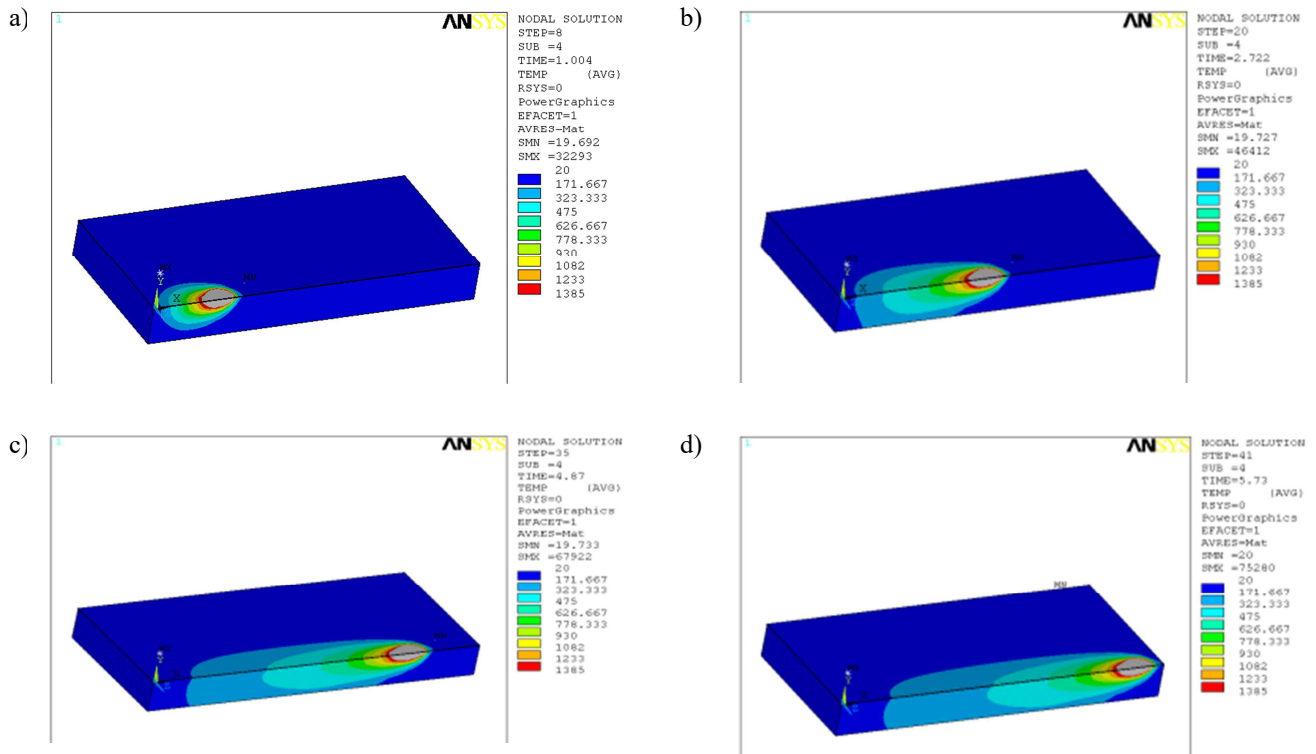


Fig. 2. Three-dimensional distribution of temperature during autogenous autogenous TIG welding at heat input 0.45 kJ/mm after: a) 1 sec, b) 3 sec, c) 5 sec and d) 7 sec

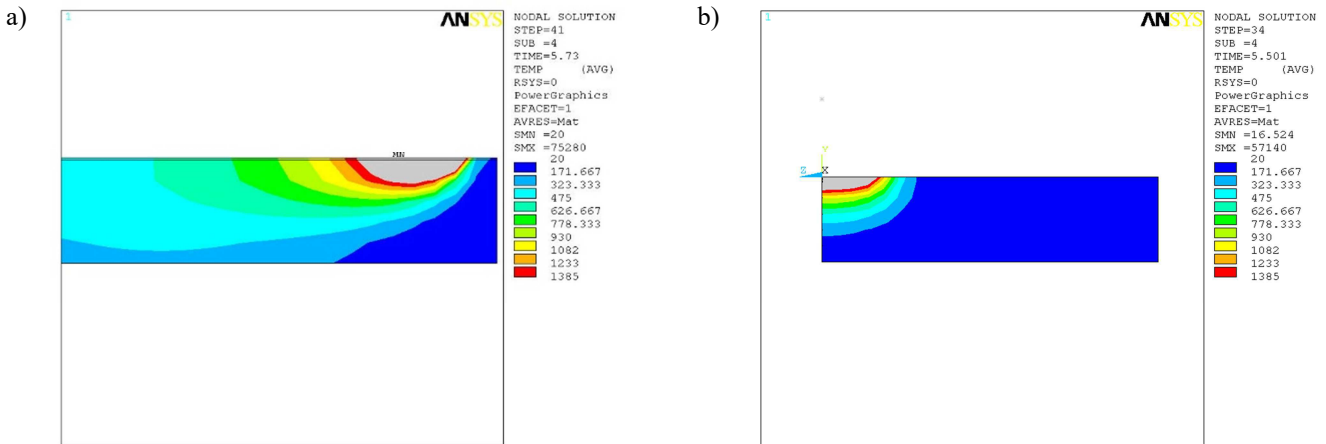


Fig. 3. Two-dimensional distribution of temperature during autogenous TIG welding at 0.45 kJ/mm after 5s; a) distribution of temperature along the length of the sample, b) the cross-section temperature distribution

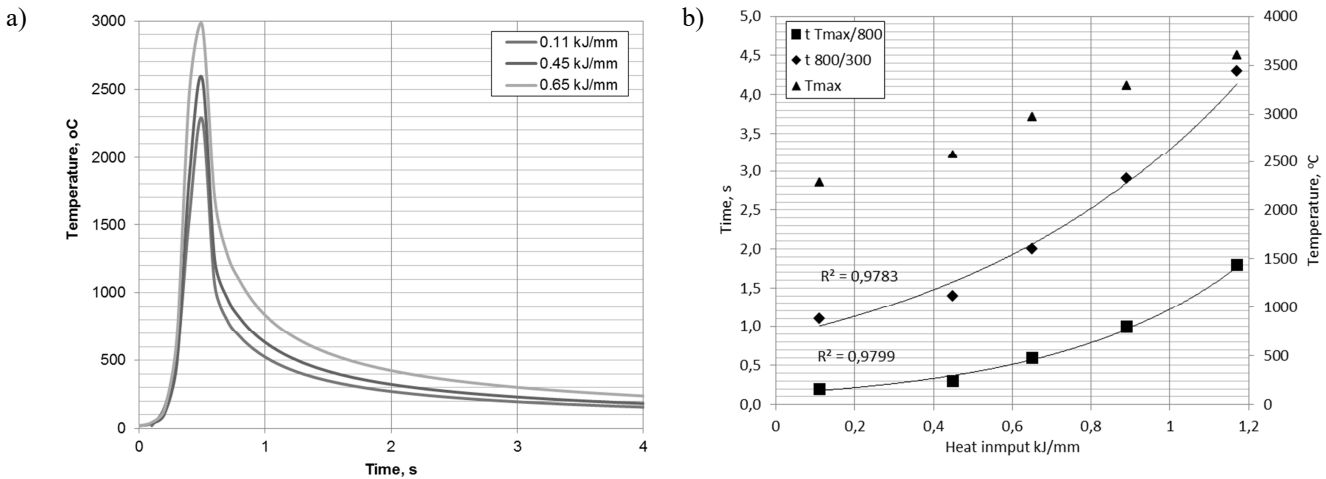


Fig. 4. Change of temperature during autogenous TIG welding at heat input 0.11÷0.45 kJ/mm: a) thermal cycle curves on measured on the surface of FEM model, b) thermal cycle parameters calculated from thermal cycle curves

The FEM model of autogenous TIG welding, provided valuable data on the heating cycle during the welding process. The Fig. 4 shows a simulation of temperature changes on selected nodes as a function of welding duration (thermal cycle curve). Analysis of the thermal cycles curves enables to determine the basic parameters such as maximum temperature (T_{max}), time to reach maximum temperature (t_{Tmax}), cooling time in the range from T_{max} to $800^{\circ}C$ ($t_{Tmax/800}$), cooling time in the range from $800^{\circ}C$ to $300^{\circ}C$ ($t_{800/300}$). Basing on thermal cycle parameters calculated from thermal cycle curves it is evident that increase of heat input in studied range influence on increase of maximum welding temperature,

while time to reach this temperature become constant 0,5 sec for 0.45 and 0.65 kJ/mm. During cooling from the welding temperature duplex microstructure is formed by the diffusion process, whereas a primary phase crystallizes ferrite and austenite precipitate on its grain boundaries and inside ferritic grains. Studied composition of lean duplex stainless steel shows Cr/Ni equivalent ratio about 4.4. The Fig. 5 shows the cross section of the Fe-Cr-Ni system with 70% Fe and indicates the percentage of the components expected for this steel after equilibrium is achieved after the welding process. During cooling ferritic microstructure pass a two phase region ($\alpha+\gamma$) where austenitic phase starts to precipitate. This phase transformation region finish

about 800°C than a complex microstructures of $\alpha+\gamma$ and σ -phase may precipitate.

Analyzing FEM thermal cycle curves and resulted parameters (Fig. 4b) most interesting regarding formation of balanced duplex microstructure was cooling time form maximum temperature to 800°C ($t_{T_{max}/800}$) that increased from 0.2 sec to 1.8 within the heat input (0.11-1.17 kJ/mm) and second parameter – cooling time in the range 800÷300°C ($t_{800/300}$) that shows higher increase form 1,1 sec at 0.11 kJ/mm to 4,1 sec at 1.17 kJ/mm. Whereas, the total cooling time form T_{max} to 300°C was varied from 1.3 to 6.1 sec. Obtained result can be correlated to measured ferrite content in the weld, thus providing a simple prediction of phase balance in weld microstructure dependent on introducing heat input.

Different configuration of welding processes were FEM simulated, i.e. MIG welding with the filler metal of duplex stainless steel composition. Fig 6. shows the temperature fields of the butt welding plates on the start of welding and after $t=10$ sec, respectively.

Residual stresses measured in welded duplex steel are caused by temperature gradients between weld zone and parent metal and by difference of thermal expansion coefficient's of ferrite and austenite phases. Due to the difference in coefficient of thermal expansion between the two phases, tensile stresses are found in the austenitic phase and balancing compressive stresses in the ferritic phase [5]. The general conclusion deriving from above for duplex stainless steels in that these alloys have a build-in resistance to cracking because the ferritic matrix is in compression and higher stresses will be required to put it

intension and cause cracking, i.e. to initiate stress corrosion cracking mechanisms [5]. Presented in the literature [6,7] residual stress measurements by neutron diffraction shows that the ferrite phase stress was tensile in the heat affected zones and weld, and appeared to be balanced by local compressive austenite phase stresses in the normal and transverse directions. Both phases shows a maximum tensile stress formed in the fill section of the weld and decreases in the root and cap regions in the transverse direction.

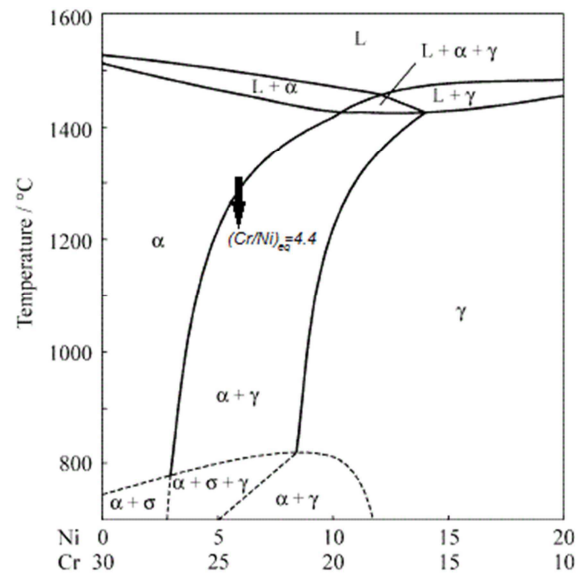


Fig. 5. The cross section of Fe-Cr-Ni system with 70% Fe [15] with marked (Cr/Ni) equivalent ratio of studied lean duplex stainless steel

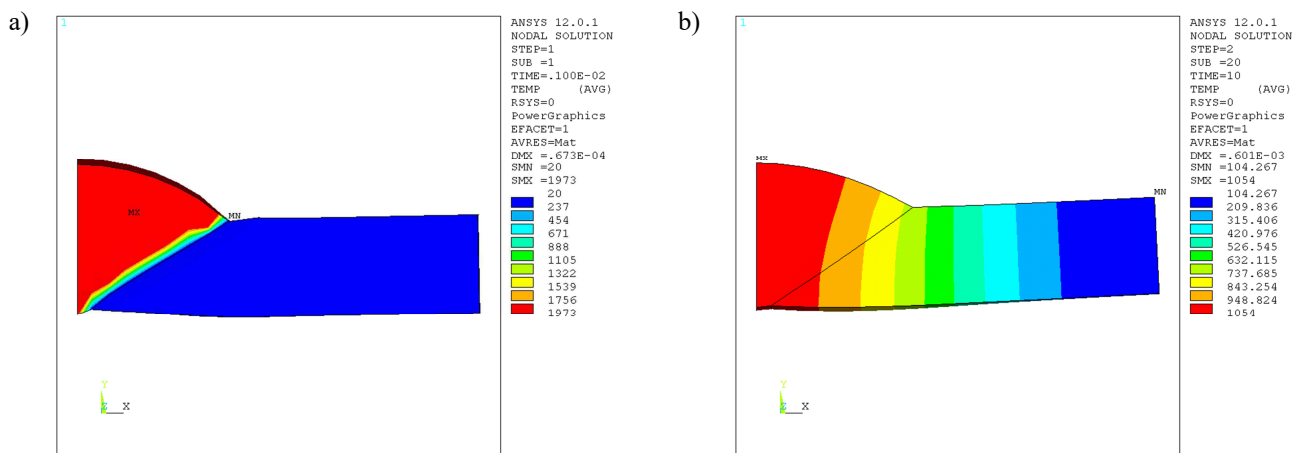
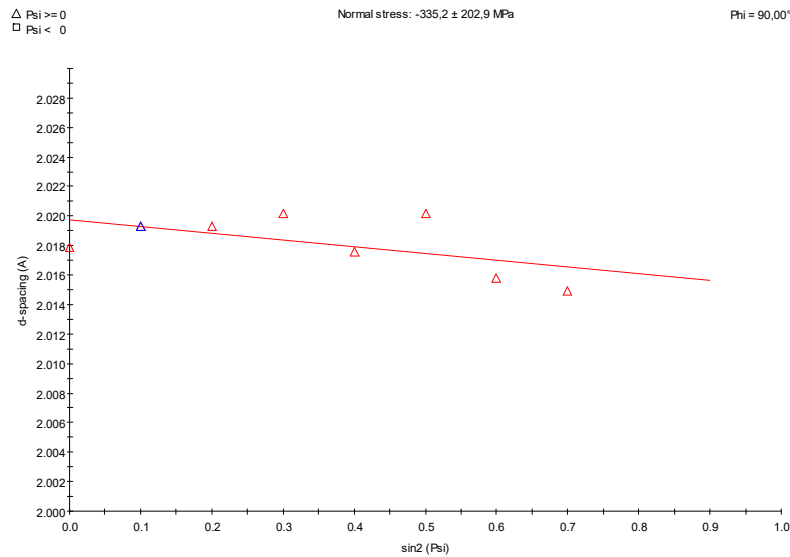


Fig. 6. The temperature fields of the butt welding plates welded at heat input 0.45 kJ/mm a) at start of welding proces and b) at $t=10$ sec

a)



b)

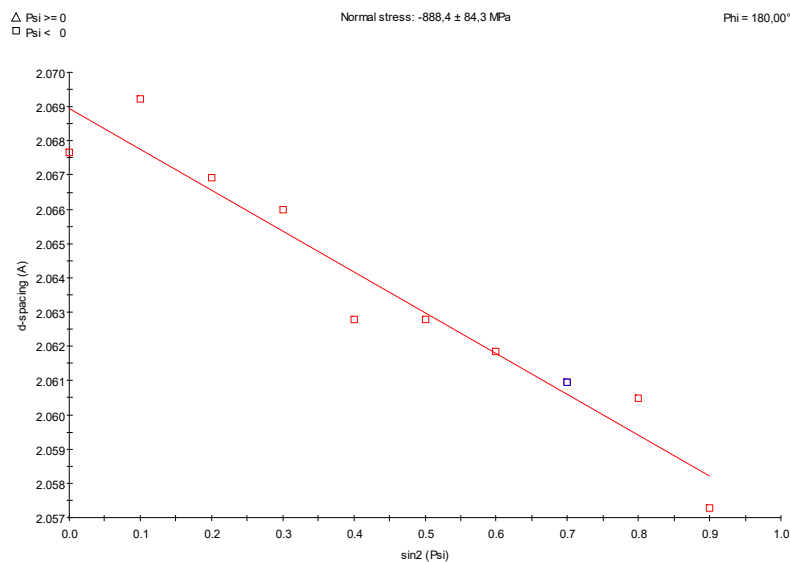


Fig. 7. Change of the a_0 value in $\sin^2\psi$ function for a) ferrite and b) austenite on the surface of weld end (surface is as weld condition)

The residual stress measurement was presented for selected systems, where autogenous TIG weld was produced and the weld surface where mechanically ground to a flat surface after welding. Machining by milling surface layer removed about 0.1 -0.3 mm (max. 0.5 mm) metal from the face of the weld. The stress analysis was then performed by mean of $g\text{-}\sin^2\psi$ method of X-ray tensometry on three surfaces: top of the face of weld, top of the face of the weld after surface machining and parent material in non-welded condition. The stress was analysed in austenite and ferrite from peak (111), respectively (Tab. 3).

Residual stress on the weld surface (the surface is as weld condition) measured at the beginning and at the end of the weld (Fig. 7) bead shows low compressive – tension (balancing) stresses in the ferritic phase, while austenite is showing high compressive stress. The machined surface in the weld bead zone shows increased compressive stress in both phases, where austenite remain more compressive stressed than ferrite. Experimental results are in good agreement with simulated FEM model (Fig. 1) regarding weld bead residual stress and its distribution on the sample surface.

Table 3.
Results of stress measurements on the welded surface calculated by means of $g\text{-sin}_2\psi$ (for ferrite α and austenite γ)

Sample	Phase	Main stress (MPa)
The beginning of weld bead – surface is as weld condition	Ferrite α	-235 \pm 100
	Austenite γ	-750 \pm 50
The end of weld bead – surface is as weld condition	Ferrite α	-335 \pm 250
	Austenite γ	-880 \pm 100
The centre of weld - surface after machining	Ferrite α	-950 \pm 100
	Austenite γ	-1400 \pm 200

4. Conclusions

Numerical calculations allow to quick selection of the optimal welding process parameters. Analysis of the thermal cycles curves has enabled to determine the basic parameters such as maximum temperature, heating time and cooling down and the rate of temperature is reached maximum and intermediate temperature ranges important for phase transformations. Simulated penetration depth and molten pool width good match the experimental results. The depth values obtained in simulation are very close to experimental data. Regarding the shape of molten pool the higher differences have been noted. The heat flux input considered in the simulation is only part of the mechanism for heating, thus the final shape of solidified molten pool will be depended strongly depend on more variables, especially the shielding gas composition, where the specific shape of the weld is obtained when using i.e. He addition to Ar atmosphere. The TIG welding (autogenous and with shielding argon and argon-nitrogen atmosphere) where a flat shape of molten pool is produced and is becoming deeper, but still having a circular shape applied FEM model is able to predict very closely the real molten pool dimensions (width and depth). Where during TIG welding a helium is applied or an activated flux (A-TIG) and penetration deep is increased as well as specific shape of molten pool is obtained applied FEM model not proven realistic comparison with the experimental data.

Comparative analysis of the numerical FEM calculations and residual stress measurements made by X-ray diffraction showed good correlation. The weld superficial residual stress (the surface is as weld condition) measured at the beginning and at the end of weld bead shows low compressive – tension (balanced) character in

the ferritic phase, while austenite is strongly compressed. The machined weld bead surface shows increased compressive stress in both phases, where austenite remain more compressive stressed than ferrite.

Acknowledgements

The author gratefully acknowledges the financial support from the National Science Centre granted based on the decision number DEC-2011/01/B/ST8/06648.

Additional information

Selected issues related to this paper are planned to be presented at the 22nd Winter International Scientific Conference on Achievements in Mechanical and Materials Engineering Winter-AMME'2015 in the framework of the Bidisciplinary Occasional Scientific Session BOSS'2015 celebrating the 10th anniversary of the foundation of the Association of Computational Materials Science and Surface Engineering and the World Academy of Materials and Manufacturing Engineering and of the foundation of the Worldwide Journal of Achievements in Materials and Manufacturing Engineering.

References

- [1] J.-S. Kim, B.-Y. Lee, W.-G. Hwang, S.-S. Kang, The Effect of Welding Residual Stress for Making Artificial Stress Corrosion Crack in the STS 304 Pipe, *Advances in Materials Science and Engineering* 932512/2015 (2015) 7.
- [2] J.-Y. Nam, D.-H. Seo, S.-Y. Lee, W.-K. Hwang, and B.-Y. Lee, The effect of residual stress on the SCC using ANSYS, *Procedia Engineering*, 10 (2011) 2609-2614.
- [3] M. Mochizuki, Control of welding residual stress for ensuring integrity against fatigue and stress-corrosion cracking, *Nuclear Engineering and Design* 237/2 (2007) 107-123.
- [4] V.I. Monin, R.T. Lopes, S.N. Turibus, J.C. Payao Filho, J. Teixeira de Assis, X-Ray Diffraction Technique Applied to Study of Residual Stresses after Welding of Duplex Stainless Steel Plates, *Materials Research* 17/1 (2014) 64-69.
- [5] R. Pettersson, E. Johansson, Outokumpu Stainless AB, Stress Corrosion Resistance of Duplex Grades,

- acom A corrosion management and applications engineering magazine from Outokumpu, 1-2011, 10-22.
- [6] B Gideon, LP Ward, Intergranular corrosion and residual stress determination of a duplex stainless steel pipeline girth weld, ARV Group, Papers and Publications, available at www.arv-offshore.com
- [7] B Gideon, L Ward, D G Carr, Strain Measurements by Neutron Diffraction and Characterization of Duplex Stainless Steel Welds, Duplex 2007 Conference, Aquileia and Grado Italy, 49, 2007.
- [8] R. Dakhlaoui, A. Baczman ski, C. Braham, S. Wronski, K. Wierzbowski, E.C.Oliver, Effect of residual stresses on individual phase mechanical properties of austeno-ferritic duplex stainless steel, *Acta Materialia* 54 (2006) 5027-5039.
- [9] L.Q. Li, Y.B. Chen, W.Y. Wang, S.Y. Lin, FEM simulation for laser forming processing. *Acta Metallurgica Sinica (English Letters)* 17 (2004) 317-322.
- [10] L. Papadakis, H. Tobias, Interaction between laser beam, process effects, and structural properties during welding using models based on the finite element analysis, *Journal of Laser Applications* 19/3 (2007) 189-196.
- [11] A. Zambon, P. Ferro, F. Bonollo, Microstructural, compositional and residual stress evaluation of CO₂ laser welded superaustenitic AISI 904L stainless steel, *Materials Science and Engineering A* 424 (2006) 117-27.
- [12] A.G. Olabi, K.Y., Benounis, M.S.J. Hashmi, Application of response surface methodology in describing the residual stress distribution in CO₂ laser welding of AISI304, *Strain* 43/1 (2007) 37-46.
- [13] H. Zeng-Rong, Z. Jian-Zhong, G. Hua-Feng, D. Jian-Jun, Simulation of temperature field of laser welding by ABAQUS, *Laser Technology* 31/3 (2007) 326-329.
- [14] Y.B. Chen, Z.L. Lei, L.Q. Li, L. Wu, Experimental study on welding characteristics of CO₂ laser TIG hybrid welding process, *Science and Technology of Welding and Joining* 11/4 (2007) 403-411.
- [15] J.W. Pugh, J.O. Niebest, *Transactions of the Metallurgical AIME* 188 (1950) 268.